X-Ray Studies of Transitions between Nematic, \(Smectic-A_1, -A_2, and -A_d\) Phases

(Article begins on next page)

X-ray studies of transitions between nematic, smectic-A_1, -A_2, and -A_d phases

K. K. Chan,* P. S. Pershan, and L. B. Sorensen[†]

Division of Applied Sciences, Harvard University, Cambridge, Massachusetts 02138

F. Hardouin

Centre de Recherche Paul Pascal, Université de Bordeaux I, 33405 Talence Cédex, France

(Received 24 January 1986)

We report high-resolution x-ray scattering measurements of the critical fluctuations in mixtures of hexylphenyl cyanobenzoyloxy benzoate (DB_6) and terephtal-bis-butylaniline (TBBA). The phase sequence exhibited on cooling pure DB_6 (or mixtures with a low concentration of TBBA), is nematic (N) to smectic-A_d (A_d) to smectic-A_2 (A_2). Mixtures with ≥ 12 molar percent (mol %) of TBBA have a smectic-A_1 (A_1) phase between the nematic and smectic-A_2 phases. For each of the second-order transitions the critical-temperature dependence of the susceptibility and correlation lengths are fit to power laws of the form t^x where $t = (T - T_c)/T_c$. For the N-A_d transition in pure DB_6 the susceptibility exponent $\gamma = 1.29 \pm 0.05$ and the parallel and perpendicular correlation-length exponents are $\nu_{||} = 0.67 \pm 0.03$ and $\nu_{\perp} = 0.52 \pm 0.03$, respectively. Close to the multicritical point (12 mol % TBBA) where the second-order N-A_1 line meets the first-order portion of the A_1-A_2 line, the N-A_1 exponents are $\gamma = 1.09 \pm 0.05$, $\nu_{||} = 0.57 \pm 0.03$, and $\nu_{\perp} = 0.43 \pm 0.03$. The correlation length anisotropy ($\nu_{||} \neq \nu_{\perp}$) persists along the entire N-A_1 line, with the observed exponents decreasing as the concentration approaches the multicritical point. The A_1-A_2 line has both first-order and second-order regions. All the measured exponents ($\gamma, \nu_{||}, \nu_{\perp}$) were invariant along the second-order portion of the A_1-A_2 line and the correlation-length exponents were isotropic ($\nu_{||} = \nu_{\perp}$). The measured exponents were $\gamma = 1.46 \pm 0.05$, and $\nu_{||} = \nu_{\perp} = 0.74 \pm 0.03$. These numbers also held close to the tricritical point where the A_1-A_2 transition became first order.

I. INTRODUCTION

At the nematic—to—smectic-A phase transition the continuous translational symmetry of the nematic phase is spontaneously broken by the appearance of a one-dimensional density wave in the smectic-A phase. Although this transition would naively appear to be the simplest solidification and/or melting transition which can occur in nature, its physics has been found to be remarkably subtle. Consequently it has been a rich subject for numerous experimental and theoretical studies. Despite these considerable efforts, it remains an unsolved problem.

The conventional smectic-A phases have been classified according to the periodicity of their one-dimensional waves. When the periodicity corresponds to the molecular length, l, the phase is called a monolayer or smectic-A_1 phase and when the periodicity corresponds to twice the molecular length, $2l$, the phase is called a bilayer or smectic-A_2 phase. There are numerous "conventional" examples of both monolayer and bilayer smectic systems that undergo continuous, or second-order, transitions between the nematic and smectic-A phases for which the critical smectic density fluctuations exhibit only a single wave vector corresponding to either the monolayer or bilayer periodicity.

Recently, a new class of polar liquid-crystal molecules were discovered[1] which exhibit a variety of new smectic phases including polar monolayer and bilayer phases and a smectic-A_d phase with a periodicity d intermediate between the monolayer and bilayer periodicity; $l < d < 2l$.

These remarkable polar smectic-A phases melt into polar nematic phases which exhibit two simultaneous fluctuations with either commensurate $d_1 = 2d_2$ or incommensurate $d_1 \neq 2d_2$ periodicities.

In this paper we report the results of a comprehensive high-resolution x-ray scattering study of these remarkable polar nematic and smectic-A phases and the transitions between them for a series of mixtures of hexylphenyl cyanobenzoyloxy benzoate (DB_6) and terephtal-bis-butylaniline (TBBA). We were motivated to study these new polar phases both because of their intrinsic interest and because they have properties that provide insight into the unsolved nematic—to—smectic-A transition. We have found that the nematic—to—smectic-A transitions in this polar system (with two simultaneous smectic fluctuations) are quantitatively different from the conventional nematic—to—smectic-A transition (in systems with a single density wave). In addition, we have found that the correlation-length exponents at the smectic-A_1 to smectic-A_2 transitions in these mixtures are isotropic, providing the first experimental support for the hypothesis that the divergent phase fluctuations of the smectic order parameter are responsible for the observed anisotropy in the nematic—to—smectic-A transition.

The next section of this paper provides a review of the experimental and theoretical background to the present work. Section III describes the experimental apparatus and techniques. Section IV presents the details of the data analysis and the experimental results. Section V provides a discussion and conclusion.

II. BACKGROUND

A. Polar smectic-A phases

The loss of translational invariance in the conventional (nonpolar) smectic-A phases is fully characterized by a single complex order parameter, $\Psi = \psi(\mathbf{r})e^{i\phi(\mathbf{r})}$, which specifies the amplitude and the phase of the one-dimensional density wave. When the constituent molecules contain strong dipole moments, the dipolar ordering can induce a second spatial period. It is convenient to describe these two possible density waves by introducing two complex order parameters. Much of the interesting physics in these systems arises from the competition between these two order parameters which, in general, have incommensurate periodicities.

Figure 1 schematically illustrates the four liquid-crystalline phases described in this study. The molecules are represented as thin rods, with an arrow at one end to denote the lack of inversion symmetry introduced by an off-center dipole. In the nematic phase the centers of mass of the molecules have fluidlike order. The molecules tend to orient with their long axis parallel to a common director $\hat{n}$, and there is a long-range molecular-orientational order. Since the nematic phase has inversion symmetry there are equal numbers of molecules pointing along $\hat{n}$ and opposite to $\hat{n}$. The smectic-A phases have a periodic density modulation parallel to the nematic director. Roughly, this can be thought of as the formation of "statistical layers" in the material. Three possible types of smectic-A phases are shown in Fig. 1. For each of

these, there is a quasi-long-range correlation between the positions of the layers. Within each layer, the molecules act like a two-dimensional fluid.

These smectic-A phases are distinguished by their layer spacings and by their dipolar order. The smectic-A_1 is a monolayer phase with the dipolar heads oriented randomly within each layer. This produces a periodicity d equal to l, the molecular length. The smectic-A_2 phase is a bilayer phase. This is attributed to a preferential up-down ordering of the dipolar heads within each layer, which alternates from layer to layer producing a periodicity d equal to twice the molecular length, $2l$. There are other systems, not studied here, that develop a further modulation parallel to the layers. This is attributed to further modulations of the head directions within the layers.[1] The smectic-A_d phase is an intermediate phase characterized by $l < d < 2l$. The dipolar heads are preferentially ordered with a slight overlap rather than end to end as in the smectic-A_2 phase. The macroscopic symmetries of the smectic-A_d and smectic-A_2 phases are indistinguishable.

The x-ray diffraction patterns of the polar nematic and polar smectic-A phases are shown in Fig. 2. The scattering for the nematic phase has two diffuse spots with wave vectors $\mathbf{q}_2 = (2\pi/l)\hat{n}$ and $\mathbf{q}_1 = q_1\hat{n}$ ($2\pi/2l \leq q_1 < 2\pi/l$) corresponding to the preferred layer spacings for monolayer and dipolar ordering, respectively. Since the wave numbers are in general incommensurate, the temperature dependence of q_1 and q_2 can be different. The presence of two strong diffuse spots in the nematic phase distinguishes these materials from the nonpolar nematic materials which have only a single diffuse spot corresponding either to the monolayer or bilayer periodicity. The smectic-A_1 phase has a Bragg-like peak at $\mathbf{q}_2$ corresponding to monolayer ordering and diffuse scattering at wave
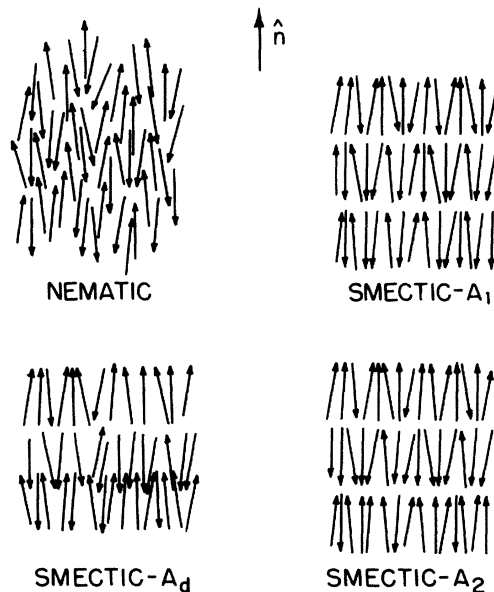

FIG. 1. Schematic representation of the polar nematic and smectic-A phases. The molecules are drawn as thin rods with an arrow on one end to denote the lack of inversion symmetry produced by an off-center dipole.

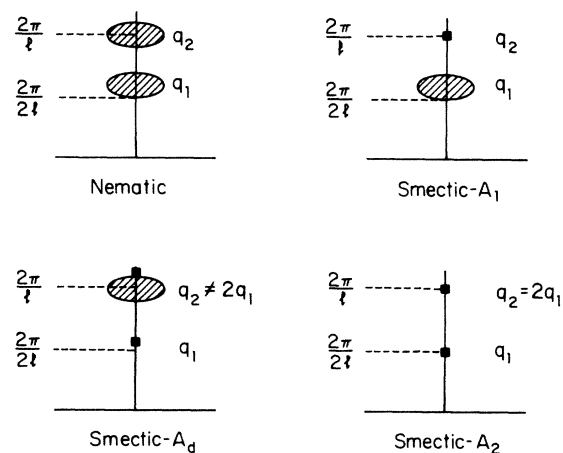FIG. 2. Diffraction patterns of the polar nematic and smectic-A phases. The vertical axis indicates the q_z direction and the horizontal axis indicates the $q_x q_y$ plane. The small solid squares denote Bragg-like spots and the large ellipses denote diffuse spots. The monolayer ordering ($d = l$) produces the scattering at q_2 and the dipolar ordering ($l < d \leq 2l$) produces the scattering at q_1.

vector q_1. The smectic-A_2 and -A_d have Bragg-like peaks at both q_1 and $2q_1$. The smectic-A_d phase also has a diffuse peak at q_2 corresponding to smectic fluctuations at the monolayer periodicity.

The first observation of a smectic-A_1—smectic-A_2 transition was made by Sigaud et al.[2] and DB$_5$-TBBA mixtures. In this paper we report studies of a similar system consisting of mixtures of DB$_6$ and TBBA. The phase diagram of DB$_6$-TBBA is shown in Fig. 3. All four of the phases discussed above are present. DB$_6$ has a strong dipolar end group and forms a smectic-A_d phase over a narrow temperature range, but primarily forms a smectic-A_2 phase. TBBA is a nonpolar molecule that forms a smectic-A_1 phase. The addition of sufficient TBBA [> 12 mole percent (mol %)] to DB$_6$ leads to a smectic-A_1 phase intermediate between the nematic and smectic-A_2 phases.

Prost and co-workers[3-6] have constructed mean-field descriptions of these phases and the corresponding phase diagrams for numerous polar smectic systems. The Prost model introduces two complex fields, Ψ_1 and Ψ_2, that order preferentially with wave numbers q_1 and q_2, respectively. This model predicts that the N-A_1 transition is a conventional N-A transition in which Ψ_2 develops quasi-long-range order (QLRO) at the transition. The model also predicts that at the A_1-A_2 transition, Ψ_1 develops in the presence of a nonzero Ψ_2 and because of a $\Psi_1^2\Psi_2^*$ coupling, the phase of Ψ_1 is locked to that of Ψ_2. Consequently, only the amplitude $|\Psi_1|$ is predicted to have critical fluctuations at the A_1-A_2 transition. The N-A_d transition is also predicted to be a conventional N-A transition where Ψ_1 develops QLRO and $|\Psi_2|/|\Psi_1|$ is small. Finally, the A_d-A_2 transition is predicted to be first-order and is characterized by a sudden change in the ratio $|\Psi_2|/|\Psi_1|$.
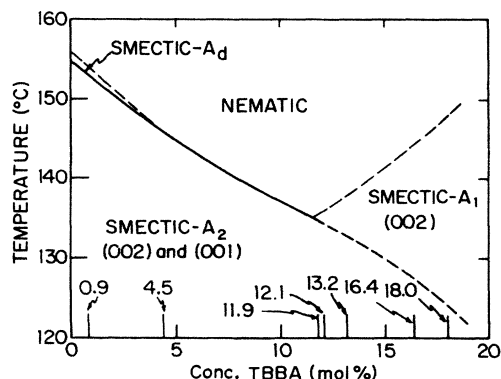

FIG. 3. Schematic phase diagram for mixtures of DB$_6$ and TBBA. The reflection at q_1 from the bilayer ordering is indexed (001) and the reflection at q_2 from the monolayer ordering is indexed (002). The dashed lines indicate second-order phase boundaries and the solid lines indicate first-order boundaries. The order of the $A_d A_2$ phase boundary has not been determined. The mixtures which were measured during this study are indicated at the bottom of the diagram.

B. Nematic—to—smectic-A transition

Since the earliest work by Kobayashi[7,8] and McMillan,[9] considerable effort has been devoted to the nematic—to—smectic-A transition. Present theories[10,11] based on the de Gennes free energy[12,13] propose two possibilities. The first is that the N-A transition is in the inverted XY class with critical exponents:[14] $\alpha=-0.02$ (specific heat); $\nu_{||}=\nu_\perp=0.67$ (correlations parallel and perpendicular to the nematic director); and $\gamma=1.32$ (susceptibility). The second possibility is an anisotropic class where $\nu_{||}=2\nu_\perp$. Unfortunately, direct comparison of the predicted XY model correlation length exponents with experiment is complicated by the absence of long-range order in the smectic-A phase.[10] Lubensky et al.[15] predict that asymptotically close to the transition, $\nu_\perp=\nu_{||}/2$ regardless of the universality class. Toner[16] predicts modified XY values of the form $\nu_{||}=\frac{6}{5}\nu_{XY}=0.80$ and $\nu_\perp=\frac{4}{5}\nu_{XY}=0.53$.

The experimentally observed correlation-lengths exponents are anisotropic with $\nu_{||}-\nu_\perp\sim0.1-0.2$ for all measured materials, and in addition are nonuniversal with $\nu_{||}$ ranging from $\sim0.6-0.8$ for different materials. Brisbin et al.[17] proposed that the apparent nonuniversality of the critical exponents is due to the presence of a nearby tricritical point. This suggestion has been confirmed by a number of studies which show that the measured critical exponents cross over from a set of "saturated values," when the nematic range is large, to a set of "tricritical values" when the nematic range is small.[18-22] Such a crossover was originally predicted by McMillan[9] to occur as the result of coupling between the nematic director fluctuations and the smectic ordering when the ratio T_{NA}/T_{NI} (called the McMillan ratio) became larger than about 0.99.

The clearest evidence for this crossover was provided by combined specific-heat and x-ray scattering studies of the critical exponents for the two homologous series, 4-n-pentylbenzenethio-4-alkoxybenzoate ($\overline{n}$S5) and alkyl-cyanobiphenyl (nCB). The crossover occurred at $n=10$ for $\overline{n}$S5 and $n=9$ for nCB. For $\overline{10}$S5 ($T_{NA}/T_{NI}=0.983$) $\alpha=0.45\pm0.05$,[17] $\gamma=1.10\pm0.05$, $\nu_{||}=0.61\pm0.03$, and $\nu_\perp=0.51\pm0.03$.[21] For 9CB ($T_{NA}/T_{NI}=0.994$) $\alpha=0.50\pm0.05$,[22] and $\gamma=1.10\pm0.05$, $\nu_{||}=0.57\pm0.03$, $\nu_\perp=0.37$ ($+0.07,-0.03$).[21] For these materials the specific-heat exponents approach the tricritical value,[23] $\alpha=0.5$, and the susceptibility exponent γ drops to 1.10 which is slightly above the tricritical value of 1.0. In addition, an average correlation length exponent $\overline{\nu}=\frac{1}{2}(\nu_{||}+\nu_\perp)$ approaches the corresponding isotropic tricritical value of 0.50. However, there is no existing theory for an anisotropic tricritial point.

The materials which are currently thought to be the most representative of true saturated N-A critical behavior have large nematic ranges (with correspondingly low McMillan ratios) and specific-heat exponents which are consistent with the predicted XY values. Two of these saturated materials are $\overline{8}$S5 and 4O.7. For $\overline{8}$S5 ($T_{NA}/T_{NI}=0.936$) $\alpha=0.0\pm0.02$, $\gamma=1.53\pm0.02$, $\nu_{||}=0.83\pm0.01$ and $\nu_\perp=0.68\pm0.02$.[17,20] For 4O.7 ($T_{NA}/T_{NI}=0.926$) $\alpha=-0.03\pm0.04$, $\gamma=1.46\pm0.03$, $\nu_{||}=0.78\pm0.02$ and $\nu_\perp=0.65\pm0.02$. [nO.7 is N-(4-n-

alkoxybenzylidene)-4-heptylaniline.] However, as originally pointed out by Garland et al.,[19] neither compound has correlation-length exponents that can be reconciled with theory.

Recently, measurements have been made of the mean-square amplitude of the order parameter near the N-A transition.[24] By fitting the experimental data to the scaling form $\langle\,|\,\Psi\,|^2\rangle = L \mp M^{\pm}\,|\,t\,|^x$ (here $M^{\pm}$ are constants above and below the transition temperatures and t is the reduced temperature) it was demonstrated that x is not equal to $1-\alpha$ as is predicted for the Landau—de Gennes free energy.[25] In addition, the discrepancy is largest for materials with long nematic ranges, which are expected to be described best by the de Gennes model. These results suggest that the Landau—de Gennes free energy must be inadequate for quantitative predictions.

C. Smectic-A_1—to—smectic-A_2 transition

Considerably less work has been done on the A_1-A_2 transition. Cursory inspection based only on the dimensionality of the system and the number of components in the order parameter would place the A_1-A_2 transition in the three-dimensional (3D) Ising class.[3] The actual situation is however more subtle, since the A_1-A_2 transition presents the novel case of a transition between two phases with QLRO. The "Ising" transition occurs on a smectic-A_1 "lattice" (with QLRO) rather than a true 3D crystal lattice (with LRO). This presents all the complications inherent in the theoretical descriptions of the smectic-A phase: QLRO, anisotropy, and coupling between the smectic layering and the nematic director. Wang and Lubensky[26] have done a renormalization-group calculation which includes all of these effects. The first order in the ϵ expansion they found that the correlation-length exponents are equal to the three-dimensional Ising value, $\nu_{||}=\nu_{\perp}=0.63$, and the susceptibility exponent γ is nonuniversal and is of order 0.1—0.2 less than the Ising value of 1.242.

Experimentally, x-ray scattering measurements on DB_6-TBBA mixtures[27] have found $\gamma=1.46\pm0.05$ and $\nu_{||}=\nu_{\perp}=0.74\pm0.03$. Heat-capacity measurements on the same system[28] found $\alpha=-0.14\pm0.06$. The two measurements are clearly consistent with the appropriate isotropic scaling law $3\nu+\alpha=2$ (experimental value 2.08 ± 0.15), but disagree with the theoretically predicted critical exponents. Recently Huse[29] proposed that the discrepancy arises because the data were taken at fixed concentration, while the theoretical values correspond to fixed chemical potential. Using the technique of Fisher renormalization[30] the expected experimental values are given in terms of the theoretical Ising values by $\gamma=\gamma_I/(1-\alpha_I)=1.24/(1-0.11)=1.39$, and $\nu=\nu_I/(1-\alpha_I)=0.63/(1-0.11)=0.71$ where the subscript I denotes the Ising values and the theoretical value[31] $\alpha_I=0.11$ is used.

III. EXPERIMENTAL

Figure 4 shows a top view of the scattering geometry and apparatus. The axes q_x and q_z define the horizontal
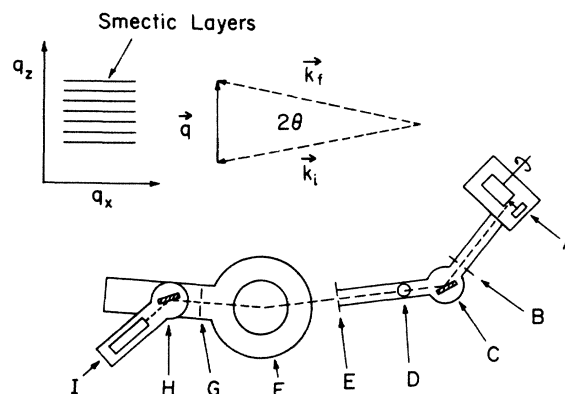

FIG. 4. Schematic diagram showing the x-ray scattering apparatus and the corresponding scattering geometry. A, rotating anode x-ray generator; B, monochromator input slits; C, germanium (220) monochromator crystal; D, incident beam intensity monitor; E, monochromator output slits; F, Huber 420 two-circle goniometer; G, analyzer input slits; H, germanium (220) analyzer crystal; I, NaI scintillation detector. The q_z direction is normal to the smectic layers and the momentum transfer is $\mathbf{q}=\mathbf{k}_f-\mathbf{k}_i$.

scattering plane. The third axis, q_y, out of this plane is referred to as the vertical direction.

The x-ray source (A) is a Rigaku RU-200 rotating anode generator operated at 4.5 kW. The monochromator input slit (B) is 2 mm wide and 25 cm from the source providing an angular collimation of about 0.5° at an angle of roughly 6° from the copper anode surface. With a 3.0 mm wide by 0.3 mm high electron focal spot, this provides an effective x-ray source size of 0.3×0.3 mm. A germanium monochromator crystal (C) cut for a (220) reflection is oriented to reflect the K_α lines of copper ($2\theta=45.2°$). For each wavelength, the Darwin width of the reflection results in an angular divergence of 3.4 mdeg full width at half maximum (FWHM) in the horizontal plane. Following the monochromator is a sheet of kapton (D) which scatters a portion of the beam vertically into a scintillation detector. This serves as a monitor for the beam intensity. The 0.06° angular dispersion of the $K\alpha_1$ and $K\alpha_2$ components ($\lambda_1=1.5406$ Å, $\lambda_2=1.5444$ Å) results in a spatial separation of these two components. Horizontal adjustment of a 1 mm wide monochromator output slit (E) located 65 cm from the source eliminates the $K\alpha_2$ component and reduces the bremsstrahlung contribution to the beam. Vertical adjustment of this slit (2 mm) determines the vertical extent of the beam incident on the sample. After exiting from the output slit, the beam passes over a Huber model 420, two-circle goniometer (F). The rotation axes of the two circles are coincident and are centered on the beam. The sample oven (90 cm from source) is mounted on one Huber circle. A rail assembly that is mounted on the second Huber circle holds the analyzer input slits (G) 20 cm from sample, a matching analyzer crystal (H) 10 cm from analyzer slit, and a scintillation detector (I) for counting the scattered x-ray photons.

The in-plane resolution of the spectrometer is determined primarily by the monochromator and analyzer crystals. The rocking curve of a pair of Ge(220) reflections has an angular width of 4.5 mdeg (FWHM). At small scattering angles, the rocking curve can be used as a first approximation for the longitudinal (along q_z) resolution. This approximation is valid only when looking at imperfectly aligned samples or diffusion scattering, as is always the case in this experiment. In addition, there is a correction for the dispersion of the natural linewidths of the copper lines. The corresponding reciprocal space resolution is 3.2×10^{-4} Å^{-1} (FWHM) in q_z, and essentially infinitely sharp in q_x. The transverse out-of-plane or vertical resolution is determined by the height of the beam at the sample (3 mm) and the analyzer input slit (8 mm vertical). These produced a 0.12-Å^{-1} (FWHM) resolution in q_y. The implications of the resolution are discussed in detail, in Sec. IV.

The liquid-crystal samples are held in a rectangular cell machined from a solid piece of beryllium (see Fig. 5). The sample thickness is 2 mm, and the illuminated scattering volume is approximately 0.5 mm wide by 3 mm high. Scattering is done in transmission. A Teflon cap is pressed against the cell to provide a seal. The cell is held in a vacuum tight, beryllium-windowed oven with two independent heating stages. The temperatures are sensed by thermistors and regulation is provided by a computer-interfaced temperature controller. The absolute temperature calibration was about 0.5 K. Typically the oven was operated with a 3—5 K temperature difference between inner and outer stages. The temperature gradient over the illuminated sample volume was measured to be less than 2 mK. Temperature stability over a period of hours was better than 1 mK. Two 2 in. diameter, 1 in. thick samarium-cobalt magnets spaced 1 in. apart in a magnetic yoke provide a 4.5-kG field for aligning the nematic

director. All measurements were done with a dry nitrogen atmosphere in the oven.

A Digital Equipment Corporation PDP 11/34 minicomputer was used to control the spectrometer angles, timing, counting, and setting and measurement of the sample temperature. The interfacing was done with a combination of CAMAC (IEEE-583) modules and GPIB (IEEE-488) instruments.

IV. EXPERIMENTAL RESULTS AND DATA ANALYSIS

Measurements were done on pure DB$_6$ and seven DB$_6$-TBBA mixtures. The concentrations studied are indicated on the phase diagram shown in Fig. 3. The five mixtures, 18.0, 16.4, 13.2, 12.1, and 11.9 mol % TBBA in DB$_6$ are to the right of the NA_1A_2 triple point in the phase diagram, and second-order N-A_1 transitions were observed. The 18.0, 16.4, and 13.2 m % mixtures are to the right of the A_1A_2 tricritical-point and second-order A_1-A_2 transitions were observed. The 12.1 and 11.0 mol % mixtures had first-order A_1-A_2 transitions. The 0.9 and 4.5 mol % mixtures were not studied in detail, but were examined to verify the topology of the phase diagram.

The organization of this section is as follows. We first present an overview of the principal structural features of the various phases of pure DB$_6$. This is followed by detailed discussions of the fitting procedures that were used to extract the correlation-length and susceptibility exponents at the N-A_d transition. After a brief discussion of the N-A_1 transition the section concludes with a longer discussion of the A_1-A_2 transition.

A. Results for pure DB$_6$

Pure DB$_6$ has a smectic-A_d phase over a narrow temperature range (~ 0.5 K) between the nematic and
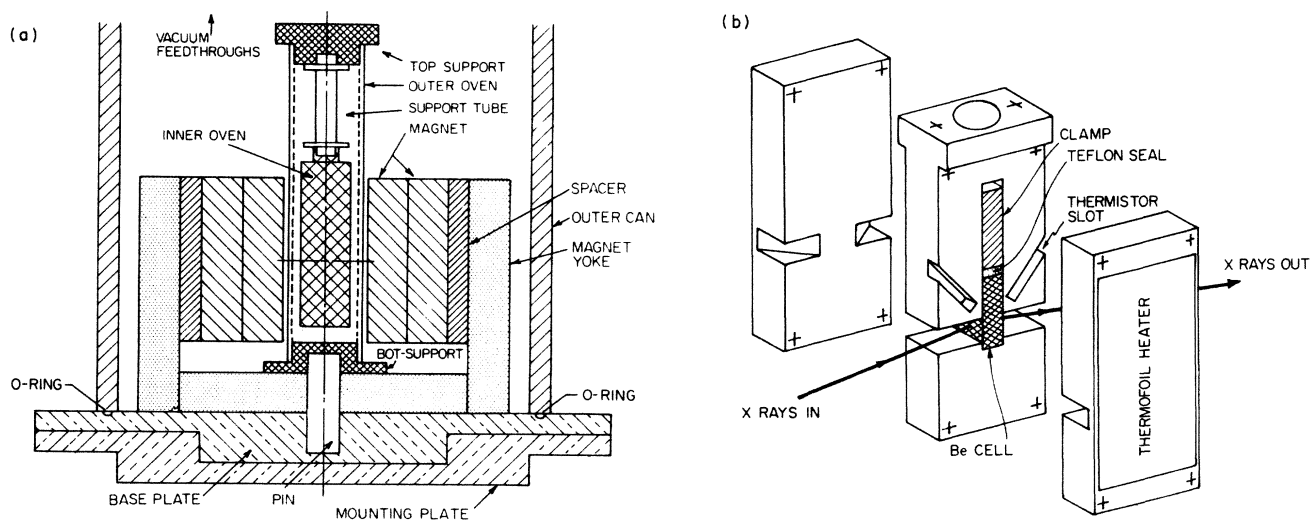

FIG. 5. Schematic diagram of the two-stage oven used in these studies. (a) Cross-sectional view of the complete oven. The magnetic field is provided by four samarium-cobalt magnets mounted in a return yoke. The outer oven is held 3—5 K below the inside oven. (b) Detail of the inner oven. The sample is sealed in a solid beryllium cell with a Teflon seal.

smectic-A_2 phases. Several degrees above the N-A_d transition, the scattering from DB_6 shows two diffuse incommensurate peaks. An (001) peak corresponding to dipolar ordering is centered at 0.1277 ± 0.0002 Å^{-1}, and an (002) peak corresponding to the monolayer ordering is centered at 0.241 ± 0.001 Å^{-1}, sightly less than twice the wave vector of the (001) peak. The width of the (002) scattering indicates longitudinal correlations of about 60 Å, or between two or three molecular lengths. The diffuse (002) scattering shows no change in shape or intensity when the temperature is lowered below the N-A_d transition temperature. The (001) peak is due to pretransitional smectic order-parameter fluctuations. These fluctuations show critical behavior and are discussed in detail below.

Below the N-A_d transition (T_{NA}), the (001) scattering is resolution limited in the longitudinal direction and mosaic limited in the transverse direction. The original diffuse (002) scattering shows no change, but a resolution-limited (002) peak appears off to one side of the diffuse scattering (Fig. 6). This resolution-limited (002) peak is at exactly twice the wave vector of the (001) smectic peak, and is first observable about 20 mK below T_{NA}. The data suggest that it is present immediately below T_{NA}, but is too weak to be seen above the diffuse scattering and background. Mosaic scans of the (001) and (002) resolution-limited scattering always showed identical structures, precluding any appreciable contribution from multiple scattering effects.[32]

In the smectic-A_d phase, the (001) wave vector q_1 changes dramatically with temperature as shown in Fig. 7. The wave vector of the resolution-limited (002) peak remains commensurate with the changing (001) wave vector at all temperatures below the N-A_d transition. The
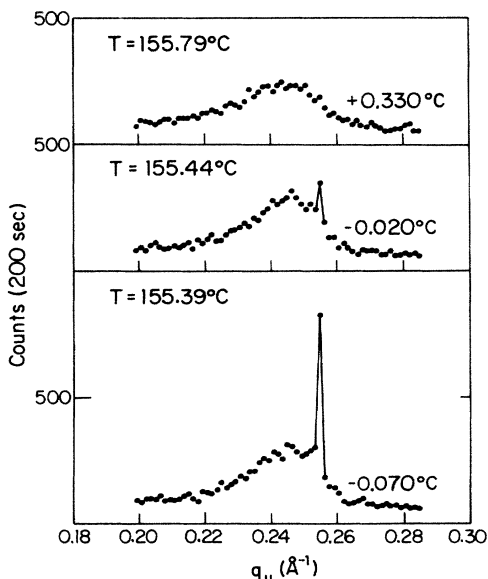
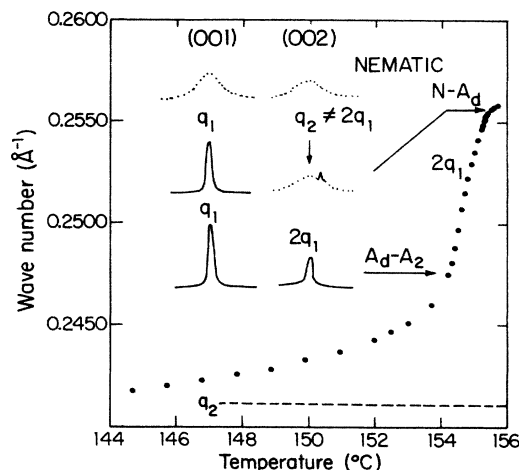

FIG. 7. Temperature dependence of the wave vectors in DB_6. The (001) peak condenses at the N-A_d transition and just below the N-A_d transition the sharp second harmonic of the (001) peak appears sightly above the center of the diffuse (002) peak. The value of $2q_1$ has been plotted in the figure to emphasize its lock in $(2q_1 \rightarrow q_2)$ at low temperature.

wave vector of the (002) diffuse scattering q_2 is temperature independent. Initially, the intensity of the resolution limited (002) peak grows slowly, as the temperature is decreased below the N-A_d transition. Then about 0.5 K below the N-A_d transition it undergoes a dramatic increase. This rapid increase is the signature of the A_d-A_2 transition. Figure 8 shows the measured intensity as a function of temperature. The sample mosaics vary rapidly with temperature due to the large changes in the smectic lattice constants. A typical mosaic width 1 K below the N-A_d transition is 4° FWHM. This variation makes it difficult to directly measure the intensity. To provide re-

FIG. 6. Longitudinal (q_z) scans showing the diffuse (002) scattering and the sharp $2q_1$ scattering near the N-A_d transition in DB_6. Finer scans of the sharp peak show that it is resolution limited. The nematic—to—smectic-A_d transition occurs at ~ 155.46 °C.
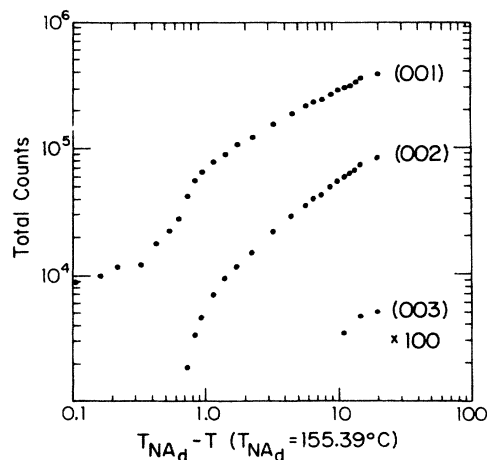

FIG. 8. Measured intensities for the resolution limited (001) and (002) scattering in the A_d and A_2 phases of DB_6. The rapid growth of the (002) peak indicates the transition to the A_2 phase. The temperatures are given relative to the N-A_d transition. The intensities were integrated over the mosaic. Deep in the A_2 phase a resolution-limited (003) peak is visible.

liable intensity data we integrated over the sample mosaic for each 2θ value. The data shown in Fig. 8 are the integrated results and were taken by heating up from the A_2 phase. Although the mosaics at low temperatures were poor, they remained relatively stable while the sample was heated, except very close (~ 50 mk) to the N-A_d transition. The data obtained from cool-down sequences showed qualitatively similar results. Deep in the A_2 phase, a weak resolution limited peak at the (003) position can be seen. This is shown in Fig. 8, magnified by a factor of 100.

In the 0.5-K region of the A_d phase, the system chooses a wave vector for the QLRO that is a compromise between the two competing wave vectors. The periodicity of the first wave vector q_1 is given by the center of the (001) fluctuations in the nematic phase which corresponds to the preferred spacing for dipolar order. The periodicity of the second wave vector q_2 is given by the center of the (003) diffuse peak, corresponding to the monolayer order. The A_d wave vector is intermediate between these two possible choices. As q_1 decreases with decreasing temperature it approaches $q_2/2$, and as the incommensuration in the system decreases, there is a transition to the A_2 phase.[6] In the A_2 phase, q_1 actually continues to change with temperature, but at a much slower rate as it approaches its low-temperature equilibrium value with $q_1 = q_2/2$ as shown in Fig. 7.

For contrast, Fig. 9 shows similar intensity measurements for DB$_5$, which has a N-A_2 transition. Calorimetry results indicate the transition is first order.[2] The x-ray data show no pretransitional fluctuation scattering on the nematic side of the transition. As the temperature is lowered two commensurate resolution-limited peaks suddenly appear and grow continuously
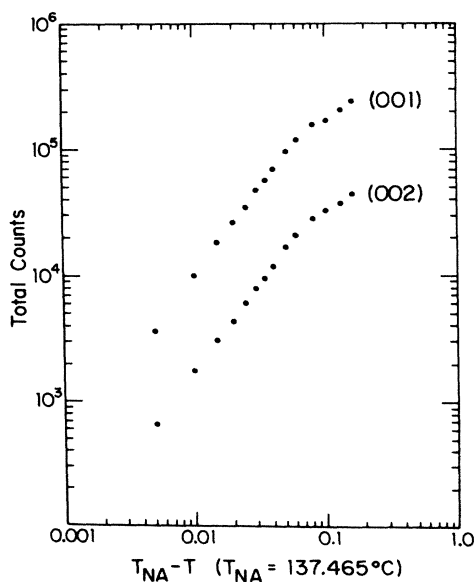
from zero intensity at the N-A_2 transition. This transition displayed a 200 mK hysteresis as expected for a first-order transition. The data shown in Fig. 9 were collected by cooling down from the nematic phase. Unlike DB$_6$, DB$_5$ does not show any dramatic changes in lattice constant below the N-A transition.

B. Data analysis and the nematic—to—smectic-A_d transition in DB$_6$

Close to the N-A_d transition, the nematic phase develops smectic order-parameter fluctuations. The scattering produced by these fluctuations are described by a modified Ornstein-Zernike expression

$$S(\mathbf{q}) = \frac{\sigma}{1 + \xi_{\|}^2(q_{\|} - q_0)^2 + \xi_\perp^2 q_\perp^2 + c\xi_\perp^4 q_\perp^4} . \tag{1}$$

The addition of the $q_\perp^4$ term in the denominator is purely phenomenological and will be discussed further below. In the smectic-A phase, the liquid crystal has Bragg-like scattering. Our instrumental resolution is unable to distinguish the subtle differences[33] between true Bragg scattering and the algebraic line shapes predicted for smectic-A liquid crystals. Consequently, the longitudinal scans are resolution limited in the smectic-A phase. As the temperature is lowered into the smectic-A phase the elastic constants increase and produce long healing lengths. As a result, competition between the alignment effects of the magnetic field and boundary conditions imposed by the walls of the beryllium cell create a polycrystalline sample. The distribution in the orientation of these macroscopic crystallites over the illuminated sample volume is the observed mosaic. The transverse scans in the smectic-A phase are limited in their width by the sample mosaic, which is always much broader than the transverse resolution. As T_{NA} is approached from below, the effect of the cell walls decreases and the alignment improves. If the magnetic field is grossly misaligned with the rectangular walls of the cell, this can lead to sudden shifts in the mosaic. Typically the mosaic widths show a minimum close to T_{NA}. The mosaics are not always smooth. Some samples displayed sharp or erratic structures such as double peaks.

In the nematic phase, the rapidly decreasing correlation lengths lead to a broadening of the scattering profile as the temperature is increased. The longitudinal scans are no longer resolution limited and the transverse widths are now dominated by fluctuation scattering instead of the sample mosaic. The transition temperature can be identified from the behavior of these linewidths. Figure 10 shows the measured linewidths for a DB$_6$ sample close to the N-A_d transition. In this case, the widths for both the longitudinal and transverse scans show no variation in the small temperature range below T_{NA}. At T_{NA} both the widths exhibit a slope discontinuity. In some samples, the mosaic width broadens slightly below T_{NA}. This leads to a cusp in the temperature dependence of the transverse FWHM's at T_{NA}. Either temperature or concentration inhomogeneities can obscure the sharpness of the cusp by
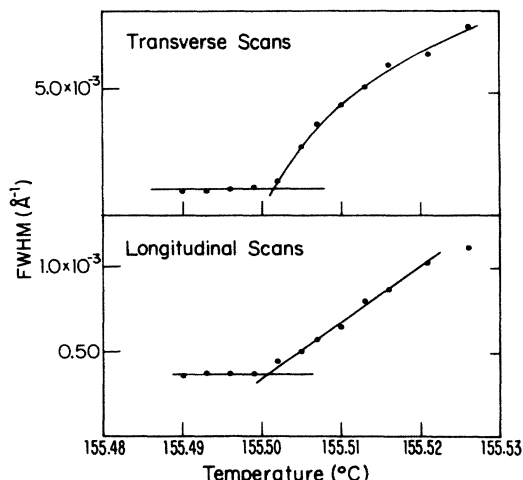

FIG. 9. Measured intensities for the resolution limited (001) and (002) scattering in the smectic-A_2 phase of DB$_5$. The intensities were integrated over the mosaic. The temperatures are given relative to the N-A_2 transition.

FIG. 10. The observed longitudinal (q_z) and transverse (q_x) linewidths (FWHM) near the N-A_d transition in DB$_6$. The transition temperature estimate from these linewidths measurements is $\sim 155.502\,°C$.

increasing the width of the narrowest transverse scan observed. Nonetheless, as shown in Fig. 10, the transition temperature can be identified to within a few mK.

The data were fitted to Eq. (1) convolved with the instrumental resolution. Longitudinal and transverse scans at each temperature were fitted together as a pair since the coarse vertical resolution (necessary to obtain adequate signal) couples the longitudinal and transverse widths. A Marquardt[34] nonlinear least-squares-fitting routine adapted from Bevington[35] was used. The free parameters are the correlation lengths $\xi_{||}$ and $\xi_{\perp}$, the susceptibility σ, the wave number q_0 and, in some cases, the quartic coefficient c.

A small absorption correction was applied to the data. In the wings of the widest transverse scans ($\pm 25°$), this amounted to an additional 10% attenuation. The thickness of the liquid-crystal sample is roughly one e length. The absorption has little effect on any of the results. A small background correction (0.15/sec) was also made.

The deviation of the structure factor from a pure Lorentzian form in the transverse direction has been reported by previous investigators. The earliest measurement was by McMillan[36] who proposed the modified form

$$S(\mathbf{q}) = 1 + \left[\beta_0 t^\gamma + \alpha_{||} \left|\frac{q_{||} - q_0}{q_0}\right|^2 + \alpha_{\perp} \left|\frac{q_{\perp}}{q_0}\right|^n \right]^{-1}. \quad (2)$$

Equation (1) follows later workers[37] in the addition of a $q_{\perp}^4$ term to the denominator. Its inclusion is necessary to obtain adequate fits to the data. For a transverse scan at a reduced temperature of 2×10^{-5}, it reduces χ^2 from 8 to 1.5. The best-fit value of c is generally in the range 0.05—0.20. Figure 11 shows least-squares fits using Eq. (1) at reduced temperatures close to and far away from the transition.

Figure 12 shows the results of the nematic correlation-length measurements for DB$_6$. The longitudinal and transverse scans at a series of temperatures were fitted in
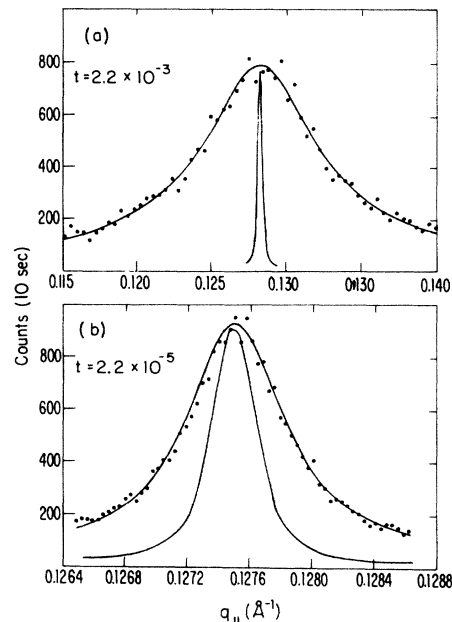

FIG. 11. Representative longitudinal (001) scans near and far from the N-A_d transition in DB$_6$. The line through the data point is the result of the least-square fits to Eq. (1) convolved with the instrumental resolution. The narrow solid line is a resolution-limited smectic-A scan.

pairs using Eq. (1). The typical values for χ^2 were 1.0—1.3. The resulting values for σ, $\xi_{||}$, and $\xi_{\perp}$ at each temperature were fitted to the power laws

$$\sigma = \sigma^0 t^{-\gamma}, \quad \xi_{||} = \xi_{||}^0 t^{-\nu_{||}}, \quad \xi_{\perp} = \xi_{\perp}^0 t^{-\nu_{\perp}} \quad (3)$$
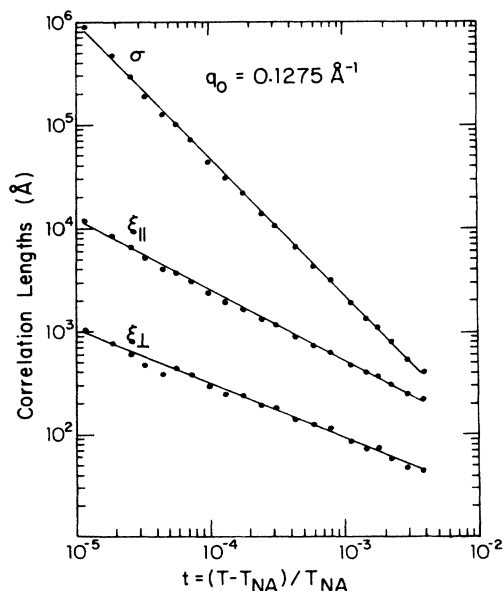

FIG. 12. Power-law fits $\sigma = \sigma^0 t^{-\gamma}$, $\xi_{||} = \xi_{||}^0 t^{-\nu_{||}}$, and $\xi_{\perp} = \xi_{\perp}^0 t^{-\nu_{\perp}}$ for the N-A_d transition in DB$_6$. The units for the susceptibility are arbitrary. For these fits T_{NA_d} was fixed at the value determined from the linewidth inspection, $T_{NA_d} = 155.502\,°C$.

[t is the reduced temperature $(T - T_{NA})/T_{NA}$]. The error bars used in the power-law fits are the statistical errors produced by the line-shape fitting program. One-standard-deviation statistical errors on the exponents were about 0.005.

One defined of Eq. (1) is that the fourth-order coefficient is not well determined. This problem is compounded by the vertical resolution. Integration over the vertical direction raises the tails observed in the in-plane scans. The fourth-order correction compensates by reducing the tails. However, χ^2 has a broad and ill-defined minimum with respect to variation in c. Thus the best-fit value varies drastically, depending on the wave-vector range covered by the transverse scan and in turn affects the best-fit value of $\xi_\perp$. The wiggles in the plot of the transverse correlation lengths (Fig. 12) are the result of this coupling.

For comparison purposes, the raw data were also fit to a variation of McMillan's form appropriately convolved with the resolution

$$S(\mathbf{q}) = \frac{\sigma}{1 + \xi_{||}^2(q_{||} - q_0)^2 + (\xi_\perp q_\perp)^{2-\eta}} , \qquad (4)$$

here both $\xi_\perp$ and $q_\perp$ are raised to $2 - \eta$. The χ^2 values for individual scan pairs remained essentially unchanged. The primary effect was on the transverse correlation lengths. At $t = 10^{-5}$, $\xi_\perp$ decreased by 20%. The effect grew progressively less at larger reduced temperatures, becoming totally negligible for $t > 10^{-3}$. The resulting effect on $\nu_\perp$ was a change from 0.51 to 0.48. The spurious oscillations in $\xi_\perp$ were reduced, but not eliminated.

Finally, the data were refit using a fixed value of c. This value was determined by averaging the values obtained for all reduced temperatures when c was left as a free parameter. This produced an increase in χ^2 for a pair of scans by at most 10% and produced no statistically significant increase in $\nu_\perp$. This effectively eliminated the troublesome oscillations. The effect on $\nu_\perp$ was about 0.01.

The data is most susceptible to artifacts at temperatures close to the transition ($t < 5 \times 10^{-5}$). Subtle errors in modeling the instrumental resolution or in locating the transition temperature can have drastic effects on these points. These systematic errors are not accounted for by the statistical weights used in the power-law fits. To estimate this systematic error, the transition temperature was varied as a free parameter. This moved the transition temperature up 1 mK from that estimated by the line-shape inspection (see Fig. 10), and caused the points closest to the transition to be consistent with the simple power-law form. This, of course, hides any crossover physics that may occur in the range $t < 5 \times 10^{-5}$. However, the readjustment of T_{NA} leaves it within the uncertainty range bracketed by the direct line-shape inspection. Consequently, the data is consistent with, and well described by, a simple power law over the entire measured temperature range.

Finally, the result of holding the value of c fixed at 0.05 and treating the transition temperature as a free parameter is shown in Fig. 13. Note that a single transition temperature results in straight lines for all three quantities
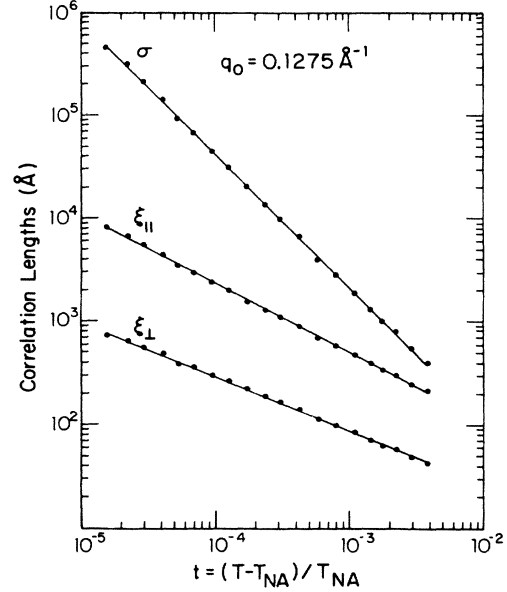

FIG. 13. Power-law fits $\sigma = \sigma^0 t^{-\gamma}$, $\xi_{||} = \xi_{||}^0 t^{-\nu_{||}}$, and $\xi_\perp = \xi_\perp^0 t^{-\nu_\perp}$ for the N-A_d transition in DB$_6$ with $c = 0.05$ and T_{NA_d} as a free parameter. The units for the susceptibility are arbitrary.

plotted, σ, $\xi_{||}$, and $\xi_\perp$

Pure DB$_6$ was found to be quite stable. The N-A_d transition temperature drifted downwards by 0.5 mK. A typical scattering measurement took about 30 h with most of the time spent far away from the transition (where the signal is weaker). The total time spent in the reduced temperature decade $t < 10^{-4}$ ($\Delta T < 40$ mK) was less than a few hours (about 20 min per temperature). The scan times for temperatures farthest away from T_{NA} were a few hours per temperature. No correction was applied for the drift in T_{NA}, but it was carefully measured at the beginning of each run. Small impurities in the sample are not believed to be important. If they are distributed homogeneously, they should simply vary the coefficients in the free energy, producing a different transition temperature. Since the basic symmetry properties of the free energy will remain unchanged, the critical exponents should remain the same. Although the N-A transition has been observed to be nonuniversal, small impurity concentrations do not produce a measurable effect on the critical exponents. The measured exponents for a given sample are always found to be independent of the small drifts in transition temperature due to sample decomposition.

Equation (1) assumes a perfectly aligned sample. If the sample has an orientational distribution in the nematic phase, the scattering from the different orientations must be included in the analysis. The mosaic distribution can be measured in the smectic-A phase by rocking the sample (mosaic scan). If the mosaic inferred from the narrowest observed mosaic scan in the smectic-A phase is assumed to hold in the nematic phase, it can be used to estimate the mosaic corrected scattering. Although the precise sample alignment at or above the transition tempera-

ture is unknown, it should depend only on the uniformity of the magnetic field. An attempt was made to include a Gaussian mosaic correction with FWHM equivalent to the narrowest smectic-A transverse scan ($\sim 0.4°$). This affected points where $1/(q_0 \xi_1)$ is less than or comparable to the mosaic angular spread (in radians). It did not improve the power-law fits, and in fact made them slightly worse. In addition, when the N-A_d transition temperature was allowed to vary, the resulting exponents became identical to the values obtained without mosaic corrections. We conclude that mosaic corrections are smaller than the precision of the present experiments.

Reasonable variations in the background and vertical resolution were also made, to estimate the corresponding systematic errors. The critical exponents for the N-A_d transition are sensitive at the level of about 0.01 to these variations. The largest variations resulted from floating the transition temperature and changing the scaling form. A total uncertainty of about 0.03 in $\nu_{||}$ and $\nu_{\perp}$, and 0.05 in γ accounts for the observed range of values produced by all these different assumptions. We use these values as our systematic error estimate. The statistical errors are negligible.

To summarize, the observed critical exponents for the N-A_d transition in DB$_6$ are

$$\gamma = 1.29 \pm 0.05 \ ,$$

$$\nu_{||} = 0.67 \pm 0.03 \ ,$$

$$\nu_{\perp} = 0.52 \pm 0.03 \ .$$

Although the combined effect of all the contributing factors affects the exponents at the level of 0.03, they are remarkably immune to larger changes. In fact, a crude estimate was done using only a pencil and a ruler and the plots of the raw data. This analysis ignored the complications due to the vertical resolution, the choice of the scaling forms, etc., and simply measured the FWHM's. The result was exponents at the bounds of the error estimates quoted above.

C. Nematic—to—smectic-A_1 transition

Correlation length measurements were done on five DB$_6$-TBBA mixtures with an N-A_1 transition (see Fig. 3). Each mixture exhibited different stability problems. They all showed N-A_1 transition temperatures that drifted downwards at typically a few mK/h. A complete characterization of the N-A_1 transition typically took from 12 to 18 hours. Short scan times were always used at the temperatures closest to the transition, where the signal is strong; 10 min per temperature was typical. The scans were started slightly below the transition temperture, and the temperature was increased in small increments past the transition. The temperature steps were then increased according to distance from the transition. Most of the data-taking time was spent far away from the transition where the signal is weak and the transition-temperature drifts are relatively unimportant.

The raw data were analyzed as described for the N-A_d transition in DB$_6$. The data were first fit to Eq. (1) with c, the coefficient of the $q_\perp^4$ term free. The data were then

refit with c fixed at the average value determined by the free fits. No mosaic correction was applied. All five mixtures showed second-order transitions. The correlation lengths obtained for each mixture are well described by power-law behavior over the entire measured temperature range. The transition temperature was treated as a free parameter in the power-law fits. It never varied by more than 3 mK from the value determined by direct line-shape inspection. No correction was made for the drifting transition temperature. Figure 14 shows the power-law fits for the 18.0 and 11.9 mol% samples. The resulting exponents for the N-A_1 transition are summarized in Table I.

D. Smectic-A_1—to—smectic-A_2 transition

Correlation-length measurements at the A_1-A_2 transition were made on the same five mixtures used for the N-A_1 transition and were reported briefly in an earlier publication.[27] The temperatures for the A_1-A_2 transition were much less susceptible to drifts than the N-A_1 transitions. The 18.0, 16.4, and 13.2 mol% mixtures exhibited second-order transitions with transition-temperature drifts of less than 1 mK/h. The 12.1 mol% mixture exhibited a weakly first-order transition and also had drifts less than 1 mK/h. The 11.0 mol% mixture had a first-order transition with about 60 mK hysteresis.

The analysis procedure for the A_1-A_2 transition differs from the N-A_1 analysis in two important ways. These are the mosaic correction and the scaling form. Unlike the N-A_1 analysis which required no mosaic correction, the A_1-A_2 definitely requires one. The A_1-A_2 transition
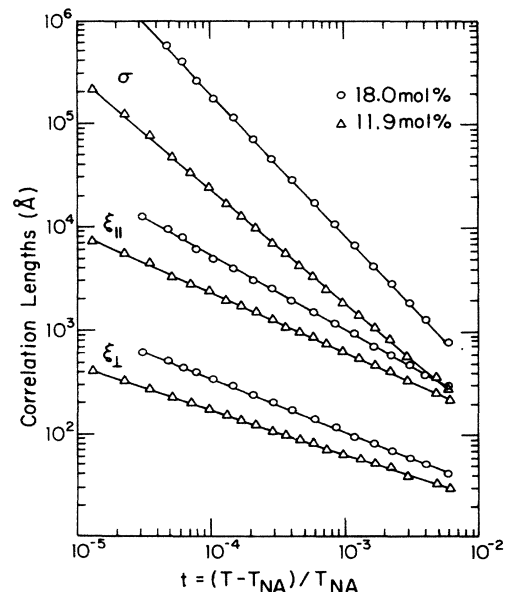

FIG. 14. Power-law fits $\sigma = \sigma^0 t^{-\gamma}$, $\xi_{||} = \xi_{||}^0 t^{-\nu_{||}}$ and $\xi_{\perp} = \xi_{\perp}^0 t^{-\nu_{\perp}}$ for the N-A_1 transition in two mixtures. For the 18 mol% mixture $q_0 = 0.2332$ Å^{-1} and for the 11.9 mol% mixture $q_0 = 0.2371$ Å^{-1}. The units for the susceptibility are arbitrary.

TABLE I. Summary of the N-A_1 power-law fits for the susceptibility $(\sigma=\sigma^0 t^{-\gamma})$, longitudinal correlation length $(\xi_\parallel=\xi_\parallel^0 t^{-\nu_\parallel})$, and transverse correlation length $(\xi_\perp=\xi_\perp^0 t^{-\nu_\perp})$ for each mixture. The units for the susceptibility are arbitrary. The reduced temperature range used in the fits was $2\times10^{-5} \leq t \leq 8\times10^{-3}$.

mol % TBBA	σ^0	γ	$\xi_\parallel^0$ (Å)	$\nu_\parallel$	$\xi_\perp^0$ (Å)	$\nu_\perp$	c
18.0	0.71	1.36[a]	7.4	0.72[b]	3.0	0.52[b]	0.05
14.4	0.84	1.30	8.6	0.69	3.1	0.49	0.08
13.2	0.69	1.27	8.5	0.67	3.0	0.48	0.09
12.1	0.93	1.16	10.4	0.62	3.5	0.44	0.09
11.9	1.0	1.09	11.8	0.57	3.3	0.43	0.09

[a]The error on the susceptibility exponent γ is ±0.05.
[b]The error on the correlation length exponents $\nu_\parallel$ and $\nu_\perp$ is ±0.03.

occurs in the presence of the ordering field of a well-developed smectic-A_1 lattice. Because of this, the sample alignment could be directly measured with a mosaic scan of the corresponding (002) smectic peak. For each sample, the smectic-A_1 crystal was "grown" by slow cooling from the nematic phase. The typical procedure was to lower the temperature several hundred mK across the N-A_1 transition over the period of an hour. The dominant features of the mosaic were found to be fully formed by about 100 mK below the N-A_1 transition. The temperature was then lowered the rest of the way to the A_1-A_2 transition (as much as 20 K lower) over a period of several hours. This could be accomplished with no serious degradation of the mosaic. Finally, cooling the temperature past the A_1-A_2 transition, into the A_2 phase, produced small changes in the mosaic distribution resulting in a growth in the tails relative to the center.

A mosaic scan for the 16.4 mol % sample is shown in Fig. 15. In the data analysis, these mosaics were modeled as Lorentzians (indicated by the solid line in the figure) out to ±8 HWHM (half width at half maximum). The

fits of the data to Eq. (1) convolved with the resolution and corrected for the mosaic gave typical χ^2 values from 1.0 to 1.5. In sharp contrast to the N-A_1 transition which always required a nonzero fourth-order coefficient, the coefficient c for the A_1-A_2 transition was always driven to zero within a statistical uncertainty many times larger than the best-fit value. Consequently, the A_1-A_2 data were analyzed without any fourth-order corrections $(c=0)$.

Figure 16 shows the results for the 18.0 and 13.2 mol % samples. Again, the transition temperature was left as a free parameter. It never varied by more than 3 mK. A 20% change in the FWHM of the mosaic distribution changed $\nu_\parallel$ and $\nu_\perp$ by about 0.01. Different assumptions about the background and vertical resolution also have ef-
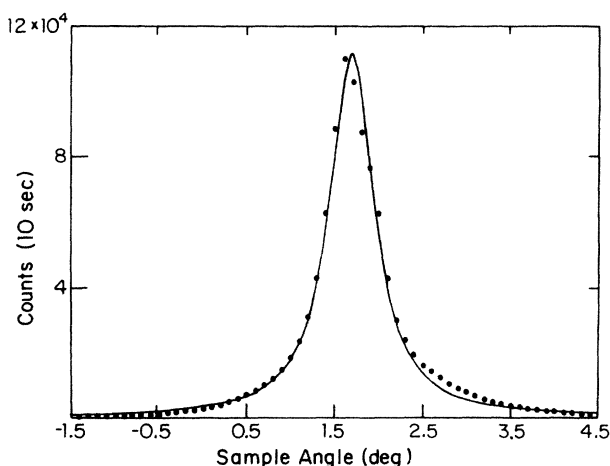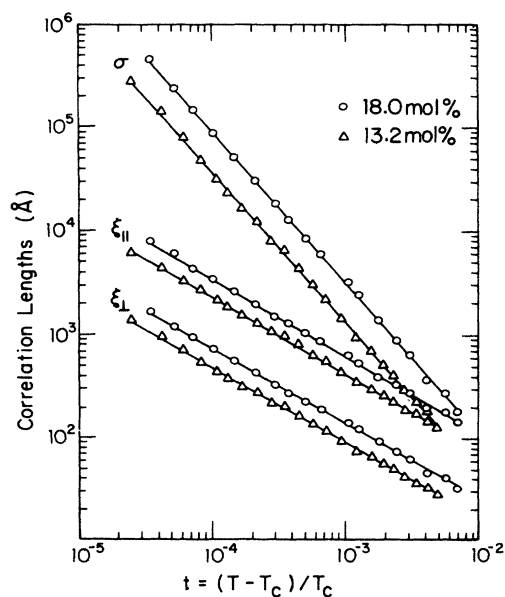

FIG. 15. Typical mosaic profile in the smectic-A_1 phase. The data points are for the 16.4 mol % mixture. The solid line indicates a Lorentzian model for the mosaic distribution.

FIG. 16. Power-law fits $\sigma=\sigma^0 t^{-\gamma}$, $\xi_\parallel=\xi_\parallel^0 t^{-\nu_\parallel}$, and $\xi_\perp=\xi_\perp^0 t^{-\nu_\perp}$ for the A_1-A_2 transition in two mixtures. For the 18 mol % mixture $q_0=0.1168$ Å^{-1} and for the 13.2 mol % mixture for $q_0=0.1179$ Å^{-1}. The units for the susceptibility are arbitrary.

TABLE II. Summary of the A_1-A_2 power-law fits for the susceptibility $(\sigma=\sigma^0 t^{-\gamma})$, longitudinal correlation length $(\xi_{||}=\xi_{||}^0 t^{-\nu_{||}})$, and transverse correlation length $(\xi_\perp=\xi_\perp^0 t^{-\nu_\perp})$ for each mixture. The units for the susceptibility are arbitrary. Except for the 12.1 mol % sample, the reduced temperature range used in the fits was $2\times10^{-5}\leq t\leq 8\times10^{-3}$. For the 12.1 mol % sample (which was weakly first order) $t>2\times10^{-4}$.

mol % TBBA	σ^0	γ	$\xi_{||}^0$ (Å)	$\nu_{||}$	$\xi_\perp^0$ (Å)	$\nu_\perp$
18.0	0.14	1.46[a]	3.5	0.75[b]	0.91	0.73[b]
16.4	0.12	1.46	3.3	0.75	0.77	0.74
13.2	0.062	1.45	2.5	0.74	0.58	0.73
12.1	(0.024)	(1.41)	(1.2)	(0.76)	(0.39)	(0.72)

[a]The error on the susceptibility exponent γ is ±0.05.

[b]The error on the correlation length exponents, $\nu_{||}$ and $\nu_\perp$ is ±0.03.

fects at this level. The results for the measured A_1-A_2 exponents are summarized in Table II. When the data for different concentrations were fit with the correlation-length exponents held fixed at the overall average value $\nu_{||}=\nu_\perp=0.74$, the ratio of the bare correlation lengths $(\xi_{||}^0$ and $\xi_\perp^0)$ were found to be independent of the TBBA concentration with $\xi_{||}^0/\xi_\perp^0\sim4$.

In the A_2 phase, the (001) and (002) Bragg-like spots were always commensurate within the instrumental resolution. This was not true in the A_1 phase where the (001) scattering was still diffuse and a slight temperature-dependent incommensuration was observed. This is shown for the 18.0 mol % sample in Fig. 17. The measured incommensuration was about 0.5%, 1 K above the A_1-A_2 transition temperature $(\xi_{||}\sim330$ Å, $\xi_\perp\sim75$ Å), and gradually decreased to zero at the transition.

V. DISCUSSION AND CONCLUSIONS

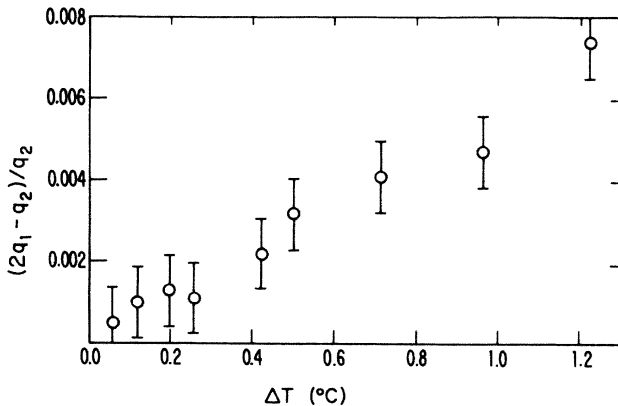In this paper we have presented the results of a comprehensive high-resolution x-ray scattering measure-

FIG. 17. Plot of the incommensurability of the (001) diffuse scattering with respect to the resolution limited (002) scattering just above the A_1-A_2 transition. The data shown are for the 18.0 mol % sample. At the transition $q_1=0.1168\pm0.0001$ Å^{-1}.

ments of the phases and phase transitions in mixtures of DB_6 and TBBA. The physics of this system is unusually rich. It contains multicritical points, commensurate-incommensurate transitions, critical phenomena, and phases with QLRO.

Our measurements on pure DB_6 have revealed a previously unobserved feature of the A_d phase—the simultaneous presence of a Bragg-like reflection at $2q_1$ and diffuse scattering at q_2 as shown in Fig. 6. This observation confirms the mean-field prediction of Barois et al.[6] which places the A_d phase in the symmetry class of the A_2 phase. The dramatic wave-vector shifts in the A_d phase and the subsequent growth in the intensity of the second harmonic at the A_d-A_2 transition is also in qualitative agreement with the mean-field-theory predictions. We also found a slower temperature-dependent shift of the wave vector in the A_2 phase as the system continued to evolve towards the original monolayer fluctuation wave vector q_2. At low temperature $2q_1\rightarrow q_2$. Taken all together, our observations lend strong support to the Prost model[5] which describes the A_d-A_2 transition in terms of the two competing order parameters. Heat-capacity measurements are now needed for this transition to confirm its first-order nature and to complete the description.

We have also measured the susceptibility and correlation-length exponents for the different second-order transitions which occur in this system. For the N-A_d transition in pure DB_6 and for the N-A_1 transition in mixtures, the exponents are for smectic-A fluctuations in the nematic phase. For the A_1-A_2 transitions, the exponents are for smectic-A_2 critical fluctuations which occur in the smectic-A_1 phase.

The measured exponents for the N-A_d transition in pure DB_6 are $\gamma=1.29\pm0.05$, $\nu_{||}=0.67\pm0.03$, and $\nu_\perp=0.52\pm0.03$. Although DB_6 has a nematic range of about 100 C, and very small McMillan ratio $(T_{NA}/T_{NI}=0.82)$, it does not exhibit the XY critical behavior which is expected in such systems.[17] It also does not exhibit the anisotropic critical exponents which have been observed in nonpolar materials (for example, $\bar{8}S5$ and 4O.7) with large nematic ranges. For pure DB_6, the measured critical exponents γ and $\nu_{||}$ agree fairly well with the XY values. However, combining the measured exponents via the anisotropic scaling relation[10] $\nu_{||}+2\nu_\perp=2-\alpha$ predicts a

specific-heat exponent $\alpha=0.29\pm0.09$, in clear disagreement with the XY value of -0.02. Although no heat-capacity measurements on DB_6 have been reported yet, this transition should definitely be studied to determine whether anisotropic scaling works in this system. This is a particularly important test since all the nonpolar materials which have been studied satisfy anisotropic scaling. The behavior observed in DB_6 clearly represents a departure from that of nonpolar materials with large nematic ranges, which have measured specific-heat exponents α close to the XY value. These discrepancies may be due to the additional degree of freedom introduced by the dipolar order parameter Ψ_2.[5,6]

Measurements on systems with a wider A_d temperature range would help to clarify this issue, as would measurements searching for possible crossover phenomena where the N-A_d line meets the N-A_2 line. Clearly, further experimental and theoretical work is needed on the role of the extra order parameter in these transitions.

The measured exponents for the N-A_1 transition are nonuniversal and anisotropy in the correlation-length exponents persists along the entire N-A_1 line. For the mixture closest to the triple point (11.9 mol% TBBA), $\gamma=1.09\pm0.05$, $\nu_{\|}=0.57\pm0.03$, and $\nu_{\perp}=0.43\pm0.03$. These values are similar to the results obtained for systems near the tricritical point[21] where the N-A transition turns first order due to the coupling between the smectic and nematic order parameters. Specifically, our susceptibility exponent γ tends toward the mean-field prediction of 1.0. In fact, it actually becomes equal to ~1.1, the value observed for the nonpolar tricritical N-A materials $\overline{10}S5$ and 9CB. In addition. the average correlation-length exponent, $\overline{\nu}\equiv\frac{1}{2}(\nu_{\|}+\nu_{\perp})$, is equal to the mean-field prediction for an isotropic transition $\nu=0.50$; just as the measured exponents for the tricritical nonpolar materials seem to approach this value ($\overline{10}S5$, $\overline{\nu}=0.56$; 9CB, $\overline{\nu}=0.47$).

The measured critical exponents for the A_1-A_2 transition are $\gamma=1.46\pm0.05$ and $\nu_{\|}=\nu_{\perp}=0.74\pm0.03$. The correlation-length exponents are isotropic within the measurement errors. This is an important result because it provides the first experimental support for the hypothesis that the divergent phase fluctuations of the smectic order parameter are responsible for the anisotropy in the N-A transition.[27] Presumably, the A_1-A_2 transition is isotropic because the Ψ_1 phase fluctuations are quenched due to lockin with the established Ψ_2 field, even though both the A_1 and A_2 phases have QLRO.

The measured critical exponents are also consistent with the measured specific-heat exponent, $\alpha=-0.14\pm0.06$[28] via the scaling law $3\nu+\alpha=2$ (experimental value 0.28 ± 0.15). Although the measured correlation-length and susceptibility exponents disagree with both the predictions for a simple Ising transition and for an Ising-like transition on a QLRO lattice,[26] they are in agreement with "Fisher renormalized" values of the simple Ising values.[30] However, the Fisher renormalized values are the asymptotic values near the transition and the theory

predicts a crossover from bare to renormalized values with decreasing reduced temperture. Since crossover effects are difficult to measure, the data often satisfy a simple power law with measured exponents that are somewhere between the bare and renormalized values. Although it is possible that the agreement between the measured and renormalized values is fortuitous, the fact that the renormalized heat-capacity exponent α_x has the opposite sign of the bare exponent α_I [i.e., $\alpha_x=-\alpha_I/(1-\alpha_I)$] supports the renormalization hypothesis. Using the theoretical Ising value, $\alpha_I=0.11$, the predicted value, $\alpha_x=-0.12$, is in reasonable agreement with the measured value $\alpha=-0.14$.

The pretransitional smectic-A_2 fluctuations in the smectic-A_1 phase were observed to be well described by a Lorentzian in both the longitudinal and the transverse directions in sharp contrast to the non-Lorentzian character of the transverse fluctuations for all known nematic—to—smectic-A transitions. This suggests that the inherent anisotropy in the N-A transition is related to the anomalous q^4 transverse tails and should provide a useful clue for future theoretical efforts. Since both γ and ν are normalized in the same way, the fact that the scaling law $\gamma=2(\nu-\eta)$ predicts an η very close to zero ($\eta=0.01\pm0.05$) implies that η is essentially zero. This contrasts with the usual anisotropic nematic—to—smectic-A transitions for which $\eta_{\perp}<0<\eta_{\|}$.

In view of the fact that this is the only example of the A_1-A_2 transition that has been studied in detail there is great need for further experiments. Although the Fisher-renormalization approach appears plausible, it may not provide the correct interpretation of the DB_6-TBBA data. For example, the A_2 fluctuation scattering was also observed to have a temperature-dependent incommensuration relative to the smectic-A_1 peak. This suggests that the coupling between the phases of Ψ_1 and Ψ_2 may not be in a "strong field" limit, and it is possible that this might be responsible for the differences between the observed exponents and the bare Ising values. Further experiments on other systems with an A_1-A_2 transition are needed to test whether the behavior observed in this system is universal or whether the A_1-A_2 transitions will exhibit the nonuniversal behavior so characteristic of the nematic—to—smectic-A transition.

The unusually rich behavior observed in the DB_6-TBBA system clearly demonstrates the intrinsic interest of the polar nematic and smectic-A phases. In addition, the observed similarities and differences between this polar system and the previously studied nonpolar systems shows the relevance of continued studies of the polar materials to the eventual resolution of the nematic—to—smectic-A enigma.

ACKNOWLEDGMENTS

*Present address: National Synchrotron Light Source, Brookhaven National Laboratory, Upton, NY 11973-5000.

†Present address: Department of Physics, University of Washington, Seattle, WA 98195.

[1]F. Hardouin, A. M. Levelut, M. F. Achard, and G. Sigaud, J. Chim. Phys. 80, 53 (1983).

[2]G. Sigaud, F. Hardouin, M. F. Achard, and H. Gasparoux, J. Phys. (Paris) Colloq. 40, C3-356 (1979).

[3]J. Prost, J. Phys. 40, 581 (1979).

[4]J. Prost, in Proceedings of the Conference on Liquid Crystals of One- and Two-Dimensional Order, Garmisch Partenkirchen (Springer Verlag, Berlin, 1980), p. 125.

[5]J. Prost and P. Barois, J. Chim. Phys. 80, 65 (1983).

[6]P. Barois, J. Prost, and T. C. Lubensky, J. Phys. 46, 391 (1985).

[7]K. Kobayashi, Phys. Lett. A 31, 125 (1970).

[8]K. Kobayashi, J. Phys. Soc. Jpn. 29, 101 (1970).

[9]W. L. McMillan, Phys. Rev. A 4, 1238 (1971).

[10]T. C. Lubensky, J. Chim. Phys. 80, 31 (1983).

[11]C. Dasgupta, Phys. Rev. Lett. 55, 1771 (1985).

[12]P. G. de Gennes, Solid State Commun. 10, 753 (1972).

[13]P. G. de Gennes, Mol. Cryst. Liq. Cryst. 21, 49 (1973).

[14]J. C. LeGuillou and J. Zinn-Justin, Phys. Rev. B 21, 3976 (1980).

[15]T. C. Lubensky, S. G. Dunn, and J. Isaacson, Phys. Rev. Lett. 22, 1609 (1981).

[16]J. Toner, Phys. Rev. B 26, 462 (1982).

[17]P. Brisbin, R. De Hoff, T. E. Lockhart, and D. L. Johnson, Phys. Rev. Lett. 43, 1171 (1979).

[18]D. L. Johnson, J. Chim. Phys. 80, 45 (1983).

[19]C. W. Garland, M. Meichle, B. M. Ocko, A. R. Kortan, C. R. Safinya, L. J. Yu, J. D. Litster, and R. J. Birgeneau, Phys. Rev. A 27, 3234 (1983).

[20]C. R. Safinya, R. J. Birgeneau, J. D. Litster, and M. E. Neubert, Phys. Rev. Lett. 47, 668 (1981).

[21]B. M. Ocko, R. J. Birgeneau, J. D. Litster, and M. E. Neubert, Phys. Rev. Lett. 52, 208 (1984).

[22]J. Thoen, H. Marynissen, and W. Van Dael, Phys. Rev. Lett. 52, 204 (1984).

[23]E. K. Riedel and F. J. Wegner, Phys. Rev. Lett. 29, 349 (1972).

[24]K. K. Chan, M. Deutsch, B. M. Ocko, P. S. Pershan, and L. B. Sorensen, Phys. Rev. Lett. 54, 920 (1985).

[25]M. E. Fischer and A. Aharony, Phys. Rev. Lett. 31, 1238 (1973).

[26]J. Wang and T. C. Lubensky, Phys. Rev. A 29, 2210 (1984).

[27]K. K. Chan, P. S. Pershan, L. B. Sorensen, and F. Hardouin, Phys. Rev. Lett. 54, 1694 (1985).

[28]C. W. Garland, C. Chiang, and F. Hardouin, Phys. Rev. A (to be published).

[29]D. A. Huse, Phys. Rev. Lett. 55, 2228 (1985).

[30]M. E. Fisher, Phys. Rev. 176, 257 (1968).

[31]G. S. Pawley, R. H. Swendson, D. J. Wallace, and K. G. Wilson, Phys. Rev. B 29, 4030 (1984), and references therein.

[32]J. Stamatoff, P. E. Cladis, D. Guillon, M. C. Cross, T. Bilash, and P. Finn, Phys. Rev. Lett. 44, 1509 (1980).

[33]L. Gunther, Y. Imry, and J. Lajzerowicz, Phys. Rev. A 22, 1733 (1980).

[34]D. W. Marquardt, J. Soc. Indust. Appl. Math. 11, 431 (1963).

[35]P. R. Bevington, Data Reduction and Error Analysis for the Physical Sciences (McGraw-Hill, New York, 1969).

[36]W. L. McMillan, Phys. Rev. A 7, 1419 (1973).

[37]D. Davidov, C. R. Safinya, M. Kaplan, S. S. Dana, R. Schaetzing, R. J. Birgeneau, and J. D. Litster, Phys. Rev. B 19, 1657 (1979).
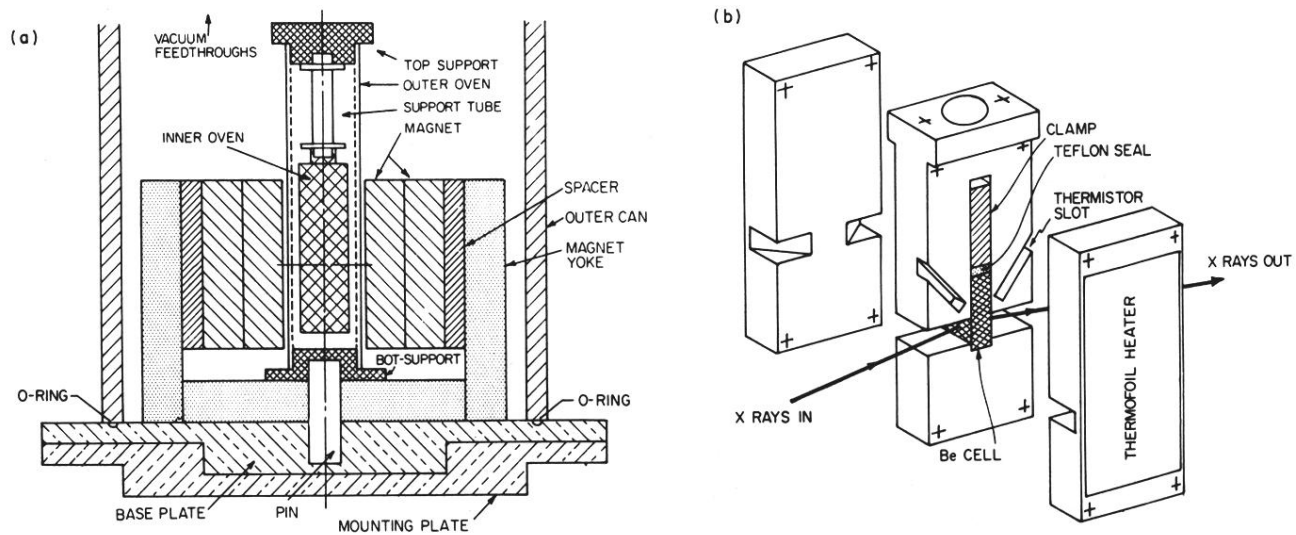
FIG. 5. Schematic diagram of the two-stage oven used in these studies. (a) Cross-sectional view of the complete oven. The magnetic field is provided by four samarium-cobalt magnets mounted in a return yoke. The outer oven is held 3—5 K below the inside oven. (b) Detail of the inner oven. The sample is sealed in a solid beryllium cell with a Teflon seal.